JOURNAL OF COMPUTATIONAL PHYSICS 97, 535–552 (1991)

A 1D Exact Treatment of Shock Waves within Spectral Methods in Plane Geometry

SILVANO BONAZZOLA AND JEAN-ALAIN MARCK

UPR 176 du C.N.R.S., D.A.R.C.,
Observatoire de Paris, section de Meudon, F-91195 Meudon Principal Cedex, France

Received June 26, 1989; revised August 27, 1990

We present a very exact numerical technique for solving 1D Euler equations coupled with the transport equations for the entropy and the chemical abundances with or without shock formation. Two moving grids are used before and after the shock formation. Quantities are expanded on both sides of the matching point in Chebychev polynomials series. After the shock is formed, Rankine–Hugoniot conditions are used to determine the velocity of the shock and the matching conditions across the shock. Typical results are presented. © 1991 Academic Press, Inc.

1. INTRODUCTION

One of the most important problems in numerical hydrodynamics is the handling of shock waves. This trouble arises in many astrophysical situations of interest, especially in simulations of gravitational collapse.

The numerical codes cannot handle shocks in a straightforward way. The existence of a shock needs a specific numerical treatment. Various methods have been developped by several authors. The most widespread are:

— finite difference codes with artificial viscocity [1]
— pseudo-spectral codes with natural viscocity [2–4]
— pseudo-spectral codes with filtering [5–8]
— Riemann solver codes [9–12].

The first two methods introduce dissipation and diffusivity of the momentum in an explicit way. Artificial viscocity, which can be roughly seen as a local modification of the equation of state is introduced in such a way that contiguous shells of matter do not cross each other. Pseudo-spectral codes with natural viscosity solve the Navier–Stokes equations with some viscous coefficient $\nu(t, x)$ which, in most practical applications, is orders of magnitude larger than the actual physical viscosity. Pseudo-spectral codes using filtering in order to smooth the high gradients and, therefore, to attenuate the Gibbs phenomenum introduce hidden diffusivity.

0021-9991/91 $3.00

The Riemann solver method solves the Riemann problem at each time step on each point of the numerical grid and then allows us to treat the shock exactly as a true discontinuity using the Rankine–Hugoniot conditions to match the solutions through the shock.

We present in this paper a pseudo-spectral numerical method which is able to treat exactly the formation and the tracking of a shock in 1D plane geometry. The method, which is described in Section 2, is general enough to solve problems in which chemical abundances must be taken into account and in which entropy production has to be considered. Our method allows us to handle shock formation and shock tracking without any kind of explicit or implicit diffusivity. This method can be seen as a generalization of a previous method which handles discontinuity formation and tracking in the Burger equation [13]. The numerical scheme is presented in Section 3. In Section 4, numerical results obtained in the case of a perfect gas are shown.

2. Equations of Motion

Consider a fluid for which the equation of states is

$$P = P(\rho, s, X_i), \tag{2.1}$$

where P is the pressure, ρ is the mass density, s is the entropy per baryon, and X_i are the chemical abundances (if any). The equations of motion can be written in the following Eulerian form:

$$\frac{\partial \rho}{\partial t} = -\frac{\partial \rho v}{\partial x} - n\frac{\rho v}{x} \tag{2.2}$$

$$\frac{\partial v}{\partial t} = -v\frac{\partial v}{\partial x} - \frac{1}{\rho}\frac{\partial P}{\partial x} - \frac{F}{\rho} \tag{2.3}$$

$$\frac{\partial s}{\partial t} = -v\frac{\partial s}{\partial x} + \Sigma_s \tag{2.4}$$

$$\frac{\partial X_i}{\partial t} = -v\frac{\partial X_i}{\partial x} + \Sigma_{X_i}, \tag{2.5}$$

where x is the spatial variable, n is an integer defining the geometry ($n = 0, 1, 2$ represents plane, cylindrical, or spherical geometry, respectively), F is a body force, and where Σ_s and Σ_{X_i} are sources, if any.

In the general case, with given initial and appropriate boundary conditions, the previous system of equations develops shocks. The spectral methods can be roughly seen as an infinite order (in space) numerical scheme when the quantities are of $\mathscr{C}^\infty$-class. However, if the quantities are of $\mathscr{C}^p$-class, spectral methods give rise to a $(p+1)$-order scheme (see, e.g., [14]). In the problem in which we are interested,

it is therefore impossible to naively use spectral methods, because the Gibbs phenomenon generated by the discontinuities of the dynamical quantities at the shock location would become so important that accuracy and convergence of the spectral approximation would be completely lost.

However, it is to be noticed that all the quantities are piece-wise $\mathscr{C}^\infty$-class, so that spectral methods lead to excellent numerical approximation of the solution on each side of the shock. Bearing in mind the previous remark and the fact that spectral methods are amenable to matching problems, we will introduce separate numerical grids on each side of the shock.

A convenient way to proceed is to rewrite Eqs. (2.2)–(2.5) as transport equations along the characteristics of the problem, namely,

$$\mathscr{C}_0 : \frac{dx}{dt} = v \tag{2.6}$$

$$\mathscr{C}_+ : \frac{dx}{dt} = (v + c) \tag{2.7}$$

$$\mathscr{C}_- : \frac{dx}{dt} = (v - c), \tag{2.8}$$

where c is the sound velocity defined as

$$c^2 = \left.\frac{\partial P}{\partial \rho}\right|_{s,\, X_i}. \tag{2.9}$$

Note that the equations for s and X_i are already written as transport equations along $\mathscr{C}_0$. Introducing the two quantities

$$I^{\pm} = v \pm N(\rho, s, X_i), \tag{2.10}$$

where N is the thermodynamic variable

$$N(\rho, s, X_i) = \int^{\rho} \frac{c}{\rho}\, d\rho, \tag{2.11}$$

the equations of evolution for ρ and v become equivalent to the following transport equations for $I^{\pm}$ along the characteristics $\mathscr{C}_+$ and $\mathscr{C}_-$:

$$\frac{\partial I^{\pm}}{\partial t} + (v \pm c)\frac{\partial I^{\pm}}{\partial x} = \left\{ c\frac{\partial N}{\partial s} - \frac{1}{\rho}\frac{\partial P}{\partial s} \right\} \frac{\partial s}{\partial x} + \left\{ c\frac{\partial N}{\partial X_i} - \frac{1}{\rho}\frac{\partial P}{\partial X_i} \right\} \frac{\partial X_i}{\partial x}$$
$$\pm \Sigma_s \frac{\partial N}{\partial s} \pm \Sigma_{X_i} \frac{\partial N}{\partial X_i} \mp n\frac{vc}{x} + \frac{F}{\rho}. \tag{2.12}$$

It is to be noted that, in the particular case of isoentropic flow ($P = P(\rho)$, $\partial s/\partial x = 0$, and $\partial X_i/\partial x = 0$), the quantities $I^{\pm}$ reduces to the usual Riemann invariants,

$$I^{\pm} = v \pm \int^{P} \frac{dP}{\rho c} \tag{2.13}$$

which, in the more particular case of pure hydrodynamics ($F = 0$) in plane geometry ($n = 0$), are constants along the characteristics $\mathscr{C}_{\pm}$ (as can be easily seen from Eq. (2.12)).

3. Grid Splitting

In this section, and in what follows, we will consider for simplicity cases where at most only one shock is present (as is the case in a spherical supernova).

Let us assume that the spatial variable x lies in the range $[a, b]$. As suggested in the previous section, we will introduce two moving numerical grids, $[a, \alpha(t)]$ and $[\alpha(t), b]$ such that, when a shock is present, $\alpha(t)$ is the space co-ordinate of the shock. Using Chebychev polynomial expansions which are defined on $[-1, +1]$, we map both the intervals $[a, \alpha(t)]$ and $[\alpha(t), b]$ onto $[-1, +1]$ by means of the following transformations:

$$\begin{aligned} x_l(t) &= \frac{2x - a - \alpha(t)}{\alpha(t) - a}; \qquad x \in [a, \alpha(t)], \\ x_r(t) &= \frac{2x - b - \alpha(t)}{b - \alpha(t)}; \qquad x \in [a, \alpha(t)]. \end{aligned} \tag{3.1}$$

Under the above transformations, the differential operators $\partial/\partial t$ and $\partial/\partial x$ become

$$\frac{\partial}{\partial t} \to \frac{\partial}{\partial t} + \frac{\dot{\alpha}}{a - \alpha}(x_l + 1)\frac{\partial}{\partial x_l}$$

$$\frac{\partial}{\partial x} \to \frac{2}{\alpha - a}\frac{\partial}{\partial x_l}$$

for $x \in [a, \alpha(t)]$, and

$$\frac{\partial}{\partial t} \to \frac{\partial}{\partial t} + \frac{\dot{\alpha}}{b - \alpha}(x_r - 1)\frac{\partial}{\partial x_r}$$

$$\frac{\partial}{\partial x} \to \frac{2}{b - \alpha}\frac{\partial}{\partial x_r}$$

for $x \in [\alpha(t), b]$.

We are then led to solve two systems of equations $(\mathscr{S}_l)$ and $(\mathscr{S}_r)$:

$$
\begin{aligned}
\frac{\partial \mathscr{I}_l^+}{\partial t} &= -(2(v_l + c_l) - \dot{\alpha}(x_l + 1)) \frac{1}{\alpha - a} \frac{\partial \mathscr{I}_l^+}{\partial x_l} \\
&\quad + \left\{ c_l \frac{\partial N_l}{\partial s_l} - \frac{1}{\rho_l} \frac{\partial P_l}{\partial s_l} \right\} \frac{2}{\alpha - a} \frac{\partial s_l}{\partial x_l} + \Sigma_{\mathscr{I}_l^+} \\
\frac{\partial \mathscr{I}_l^-}{\partial t} &= -(2(v_l - c_l) - \dot{\alpha}(x_l + 1)) \frac{1}{\alpha - a} \frac{\partial \mathscr{I}_l^-}{\partial x_l} \\
&\quad + \left\{ c_l \frac{\partial N_l}{\partial s_l} - \frac{1}{\rho_l} \frac{\partial P_l}{\partial s_l} \right\} \frac{2}{\alpha - a} \frac{\partial s_l}{\partial x_l} + \Sigma_{\mathscr{I}_l^-} \\
\frac{\partial s_l}{\partial t} &= -(2v_l - \dot{\alpha}(x_l + 1)) \frac{1}{\alpha - a} \frac{\partial s_l}{\partial x_l} + \Sigma_{s_l} \\
\frac{\partial X_{il}}{\partial t} &= -(2v_l - \dot{\alpha}(x_l + 1)) \frac{1}{\alpha - a} \frac{\partial X_{il}}{\partial x_l} + \Sigma_{X_{il}} \\
\frac{\partial \mathscr{I}_r^+}{\partial t} &= -(2(v_r + c_r) - \dot{\alpha}(x_r - 1)) \frac{1}{b - \alpha} \frac{\partial \mathscr{I}_r^+}{\partial x_r} \\
&\quad + \left\{ c_r \frac{\partial N_r}{\partial s_r} - \frac{1}{\rho_r} \frac{\partial P_r}{\partial s_r} \right\} \frac{2}{b - \alpha} \frac{\partial s_r}{\partial x_r} + \Sigma_{\mathscr{I}_r^+} \\
\frac{\partial \mathscr{I}_r^-}{\partial t} &= -(2(v_r - c_r) - \dot{\alpha}(x_r - 1)) \frac{1}{b - \alpha} \frac{\partial \mathscr{I}_r^-}{\partial x_r} \\
&\quad + \left\{ c \frac{\partial N_r}{\partial s_r} - \frac{1}{\rho_r} \frac{\partial P_r}{\partial s_r} \right\} \frac{2}{b - \alpha} \frac{\partial s_r}{\partial x_r} + \Sigma_{\mathscr{I}_r^-} \\
\frac{\partial s_r}{\partial t} &= -(2v_r - \dot{\alpha}(x_r - 1)) \frac{1}{b - \alpha} \frac{\partial s_r}{\partial x_r} + \Sigma_{s_r} \\
\frac{\partial X_{ir}}{\partial t} &= -(2v_r - \dot{\alpha}(x_r - 1)) \frac{1}{b - \alpha} \frac{\partial X_{ir}}{\partial x_r} + \Sigma_{X_{ir}}
\end{aligned}
\tag{3.2}
$$

with appropriate boundary conditions on a and $\alpha(t)$ for $(\mathscr{S}_l)$ and on $\alpha(t)$ and b for $(\mathscr{S}_r)$.

3.1. *Pre-shock Treatment*

When no shock is present, every quantity is continuous and α may be an arbitrary function of time under the condition $\alpha(t_{\text{shock}}) = x_{\text{shock}}$. However, from a numerical point of view, it is convenient, but not necessary, that the relative velocity of the fluid with respect to the grid on $x = \alpha(t)$ is subsonic, i.e., $|\dot{\alpha}(t)| < c(\alpha(t))$. The method we recommend will be described in the following section.

The problem becomes well-posed once initial conditions and appropriate boundary conditions on a, $\alpha(t)$, and b are given. The initial conditions are arbitrary. However, the way in which the boundary conditions are introduced is strongly constrained by the directions of the three characteristics $\mathscr{C}_0$, $\mathscr{C}_+$, and $\mathscr{C}_-$ issued from a, $\alpha(t)$, and b. Let us consider for simplicity the case where $|v| < c$ on a and b. The diagram of the characteristics is shown on Fig. 1a. It follows that on the left side ($x \in [a, \alpha(t)]$):

One boundary condition must be imposed on s and X_i on $x = a$ ($x_l = -1$) if and only if $\mathscr{C}_0(a)$ is ingoing ($v(a) > 0$).

One boundary condition must be imposed on s and X_i on $x = \alpha(t)$ ($x_l = +1$) if and only if $\mathscr{C}_0(\alpha)$ is ingoing ($v(\alpha) < \dot{\alpha}$).

One boundary condition must be imposed on I^+ on $x = a$ ($x_l = -1$). One boundary condition must be imposed on I^- on $x = \alpha$ ($x_l = +1$).

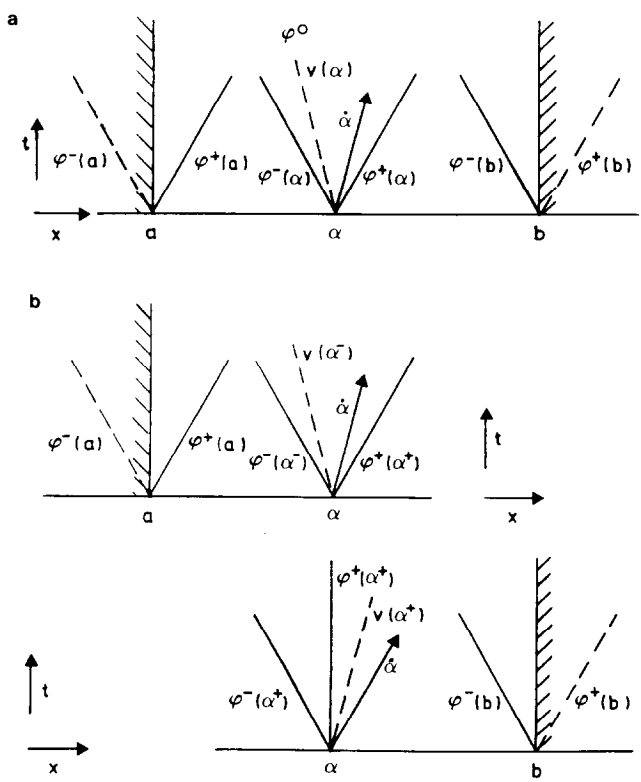

FIG. 1. Shape of the characteristics $\mathscr{C}_0$, $\mathscr{C}_+$, and $\mathscr{C}_-$ issued from the points a, α and b (a) when no shock is present; (b) the relative position of the tangent to the shock path with respect to the characteristics when a shock is present on α.

Remember that, under the above assumptions, $\mathscr{C}_+(a)$ is always ingoing and $\mathscr{C}_+(\alpha)$ is always outgoing, and, in the same way, $\mathscr{C}_-(a)$ is always outgoing and $\mathscr{C}_-(\alpha)$ is always ingoing.

Similar rules apply to the way in which boundary conditions are treated for $\mathscr{S}_r$, namely $x \in [\alpha(t), b]$.

The values of the boundary conditions on $x = a$ and $x = b$ are arbitrary. However, for $x = \alpha(t)$, the boundary conditions on $x = \alpha(t)$ for $\mathscr{S}_l$ and $\mathscr{S}_r$ have to be determined in such a way that the global solution is continuous on $\alpha(t)$, i.e.,

$$s_l, X_{il}, I_l^+, I_l^-|_{x_l=+1} = s_r, X_{ir}, I_r^+, I_r^-|_{x_r=-1}. \tag{3.3}$$

Note that the above considerations can be generalised to the case $|v(a)| > c(a)$ or/and $|v(b)| > c(b)$.

3.2. *Post-shock Treatment*

Once the shock is formed, the way in which boundary conditions are treated does not change. But, since the relative velocity of the fluid with respect to the velocity of the shock is supersonic on one side of the shock and subsonic on the other side, the matching conditions on $x = \alpha(t)$ are different. We recall that now $\alpha(t)$ is the position of the shock and $\dot{\alpha}(t)$ is its velocity.

Let us assume without loss of generality that the supersonic region is the right side of the shock, that is,

$$|v(\alpha^+) - \dot{\alpha}| > c(\alpha^+)$$

and

$$|v(\alpha^-) - \dot{\alpha}| < c(\alpha^-). \tag{3.4}$$

Then there is no ingoing characteristic issued from α^+ into the right side of the shock (see Fig. 1b). Consequently, the system of equations $\mathscr{S}_r$ must be integrated without any boundary condition on $x = \alpha^+$ $(x_r = -1)$.

On the other hand, the system of equations $\mathscr{S}_l$ must be integrated with boundary conditions on $x = \alpha^-$ $(x_l = +1)$ for s_l, X_{il}, and I_l^-. Non-accumulation of energy, mass, chemical abundances, and momentum on the shock implies generalized Rankine–Hugoniot relations. These relations allow us to determine the values of the boundary conditions for s_l, X_{il}, and I_l^- and to determine the velocity of the shock, namely $\dot{\alpha}(t)$.

4. Determination of α

As explained in the preceeding section, before a shock is formed, $\alpha(t)$ can be any arbitrary function of time under the conditions

$$\begin{aligned} &|\dot{\alpha}(t)| < c(\alpha(t)); && t < t_{\text{shock}} \\ &\alpha(t) = x_{\text{shock}}(t); && t \geqslant t_{\text{shock}}, \end{aligned} \tag{4.1}$$

where x_{shock} is the space co-ordinate of the shock, and where t_{shock} is the time of the birth of the shock.

A shock forms when and where $(\mathscr{C}_+, \mathscr{C}_-)$ leaves off being an admissible coordinate system, that is, when and where neighbouring characteristics of the same kind ($\mathscr{C}_+$ or $\mathscr{C}_-$) intersect each other. Consequently, at each time t, it is possible in principle to determine from the knowledge of all the quantities the shape of the characteristics, and then t_{shock} and x_{shock}.

The above properties are used to compute $\alpha(t)$. At each time-step t^J, for each couple of sampling points (x_i, x_{i+1}), we solve the system of equations in $x_i^{\pm}$ and $t_i^{\pm}$

$$\begin{aligned} x_i^{\pm} - x_i &= (v(x_i, t^J) \pm c(x_i, t^J))(t_i^{\pm} - t^J) \\ x_i^{\pm} - x_{i+1} &= (v(x_{i+1}, t^J) \pm c(x_{i+1}, t^J))(t_i^{\pm} - t^J), \qquad i = 1, \ldots, N-1, \end{aligned} \tag{4.2}$$

where N is the number of grid points.

The solution of this system gives a set of $2(N-1)$ points $P_i^{\pm}$. Among the points $P_i^{\pm}(t_i^{\pm}, x_i^{\pm})$ satisfying

$$t_i^{\pm} \geqslant t^J, \tag{4.3}$$

we choose the point $C(t_0, x_0)$ such that

$$t_0 = \text{Min}\{t_i^{\pm}\}. \tag{4.4}$$

The co-ordinates of this point give a forecast of the time and the position of the shock's birth. Note that this method would give the exact value of t_{shock} and

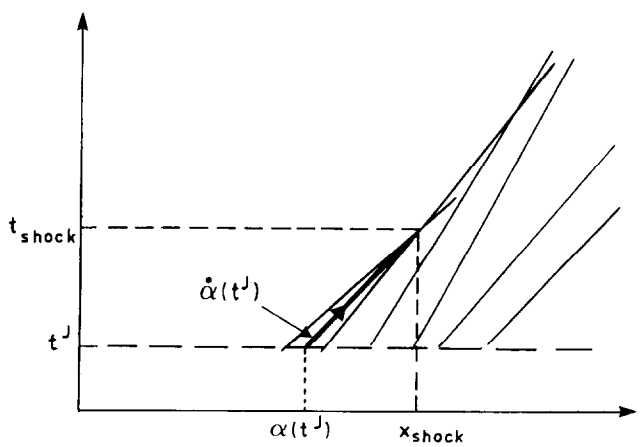

FIG. 2. Geometrical prediction of the two-position of the shock in the space (t, x) and computation at the time t^J of $\dot{\alpha}$.

$x_{\text{shock}}(t_{\text{shock}})$ when $x_i - x_{i+1}$ goes to zero and when v and c are constant along the characteristics; α is then integrated forward in time by means of

$$\alpha(t^{J+1/2}) = \alpha(t^{J-1/2}) + \dot{\alpha}(t^J)\, dt, \tag{4.5}$$

where

$$\dot{\alpha}(t^J) = \frac{x_0 - \alpha(t^J)}{t_0 - t^J}. \tag{4.6}$$

Figure 2 shows how $\dot{\alpha}$ is computed.

At the first step, $\alpha(0)$ is chosen in such a way that $\alpha(t)$ is always $(t \leqslant t_{\text{shock}})$ inside the influence cone issued from $(t_{\text{shock}}, x_{\text{shock}})$.

Note that this method gives an accuracy increasing with time for the evaluation of $(t_{\text{shock}}, x_{\text{shock}})$ because when $t_{\text{shock}} - t^J$ becomes smaller and smaller, then the affine approximation (4.2) becomes, of course, better and better.

5. Numerical Scheme

We want to emphasise that we perform numerical integration of the coupled systems $\mathscr{S}_l$ and $\mathscr{S}_r$ along the co-ordinates (x_l, t) and (x_r, t), respectively. Numerical integration along the characteristics $\mathscr{C}_+$ and $\mathscr{C}_-$ cannot be used when a shock happens because the co-ordinate system $(\mathscr{C}_+, \mathscr{C}_-)$ becomes singular.

We use Chebychev polynomial expansions to approximate physical quantities. We recall that this approximation gives rise to a great accuracy in the computational of spatial derivatives, allows a fast algorithm, and is well suited to treat non-periodic boundary condition problems. Moreover, the canonical numerical grid associated with Chebychev polynomials is oncentrated near the boundary of the interval ($\Delta x \propto 1/N^2$, where N is the number of degrees of freedom) which is useful for approximating functions that are stiff near the boundaries. See, for instance, Gottlieb and Orszag [14] or Canuto *et al.* [15].

5.1. *Integration Forward in Time*

A second-order temporal numerical scheme is used. The numerical integration is performed in a semi-implicit way in order to avoid the Courent condition which can become very severe near the boundaries because of the high density of the sampling points. We have to solve transport equations for which the general form is

$$\frac{\partial f}{\partial t} = -w(t, x, f)\frac{\partial f}{\partial x} + \text{Source}_f \tag{5.1}$$

The numerical temporal scheme is

$$f^{J+1} = f^J + dt \times \left\{ (-w^{J+1/2} + c_1 x + c_2) \frac{\partial f^{J+1/2}}{\partial x} - \frac{1}{2}(c_1 x + c_2) \frac{\partial f^{J+1}}{\partial x} - \frac{1}{2}(c_1 x + c_2) \frac{\partial f^J}{\partial x} + \text{Source}_f^{J+1/2} \right\}, \tag{5.2}$$

where superscript J, $J+1/2$, and $J+1$ refer to times $t = t^J$, $t^{J+1/2} = t^J + dt/2$, and $t^{J+1} = t^J + dt$. The quantities computed at the time $t^{J+1/2}$ are evaluated by extrapolation of their values at the times t^{J-1} and t^J. The coefficients $c_1(t)$ and $c_2(t)$ are determined in such a way that $w - c_1 x - c_2$ vanishes at the boundaries at the time t^J.

The previous equation written in the Chebychev representation reads

$$\tilde{f}_l^{J+1} = \tilde{f}_l^J + \frac{dt}{2} \mathscr{D}_{lm} \tilde{f}_m^{J+1} + \frac{dt}{2} \mathscr{D}_{lm} \tilde{f}_m^J + dt\, \mathscr{N}_l^{J+1/2}, \tag{5.3}$$

where $\tilde{f}_l$ and $\mathscr{N}_l$ are the coefficients of the Chebychev expansion of f and of all the quantities computed at the time $t^{J+1/2}$ and where $\mathscr{D}_{lm}$ are the matrix coefficients of the operator $(c_1 x + c_2)\, \partial/\partial x$. Note that the solution of the above algebraic system is easily obtained, because the matrix $\mathscr{I} - \mathscr{D}$ can be simply reduced to a tridiagonal matrix (see, e.g., [2, 3]).

In the case of a system of M coupled partial differential equations, the above algebraic system becomes a system $\mathscr{S}_{N \times M}$ of $N \times M$ coupled equations, where N is the number of degrees of freedom. However, if the values of the boundary conditions are known at the time t^{J+1} for each quantity, it can be seen from the numerical scheme used, (5.2), that the system $\mathscr{S}_{N \times M}$ reduces to M decoupled systems of N equations.

5.2. *Boundary Condition Problem*

The determination of the value of the boundary condition which has to be applied to some quantity Q at the time t^{J+1} can be seen as a viscious circle. Consider, for instance, the problem of finding the boundary values of $\mathscr{I}_l^+$ and $\mathscr{I}_l^-$ on the matching point α in the simple case $v(t, a) = v_a$ and $v(t, b) = v_b$ ($|v_a| < c(a)$ and $|v_b < c(b)$) when no shock is present.

The previous boundary conditions read

$$\mathscr{I}_l^+(-1) + \mathscr{I}_l^-(-1) = 2v_a \tag{5.4}$$

$$\mathscr{I}_r^+(+1) + \mathscr{I}_r^-(+1) = 2v_b \tag{5.5}$$

$$\mathscr{I}_l^+(+1) = \mathscr{I}_r^+(-1) \tag{5.6}$$

$$\mathscr{I}_l^-(+1) = \mathscr{I}_r^-(-1). \tag{5.7}$$

Taking into account that the integration in time is performed simultaneously on the left and on the right numerical grids it appears that it is not possible to determine the values of $\mathscr{I}^+$ and $\mathscr{I}^-$ at the boundaries at the time t^{J+1}. Indeed, the boundary value of $\mathscr{I}^+$ at the time t^{J+1} depends on the value of $\mathscr{I}$ at the time t^{J+1} and vice versa. Note that the algebraic system (5.3) can be generalised in a straightforward way for solving M $(M>1)$ equations. In this case, the problem of the boundary values disappears, but the matrix $\mathscr{I}-\mathscr{D}$ becomes a $M\times N$ squared matrix. This method has been successfully used for the resolution of the 1D Burger equation with viscosity on two or three moving grids by Macaraeg and Street [4] but becomes prohibitive and cumbersome to code when $M>1$.

Noted that Euler equations are hyperbolic, and, consequently, the signal velocity is finite (unlike the Navier–Stokes equations for which the signal velocity is infinite). We use this property to solve the boundary condition problem in the following way.

We first perform a numerical integration for $\mathscr{I}_l^+$ on the left side with an arbitrary boundary condition on $x=a$ which leads to a provisional solution $\mathscr{I}_{lw}^+$, say. Note that, because of the hyperbolicity of the equations, the boundary condition influences the solution only on the interval $[a, (v+c)\,dt]$ and, consequently, $\mathscr{I}_{lw}^+$ is the exact value of $\mathscr{I}_l^+$ at the time t^{J+1} on the interval $[(v+c)\,dt, \alpha]$. The value at $\mathscr{I}_{lw}^+(\alpha)$ and the matching condition on α give the desired boundary condition for the numerical integration of $\mathscr{I}_r^+$. The boundary condition $v(t, b)=v_b$ with the value of $\mathscr{I}_r^+(b)$ at the time t^{J+1} gives the expected boundary condition on $x=b$ for $\mathscr{I}_r^-$. After the integration of $\mathscr{I}_r^-$, we use the matching condition on α and the value $\mathscr{I}_r^-(\alpha)$ at the time t^{J+1} to determine the value of the boundary condition requested for the integration of $\mathscr{I}_l^-$. Now, we can determine the exact value of the boundary condition on $x=a$ for $\mathscr{I}_l^+$ by means of the given boundary condition $v(t, a)=v_a$ and of the value of $\mathscr{I}_l^-(a)$ at the time t^{J+1}, and, consequently, integrate $\mathscr{I}_l^+$.

6. Numerical Results

In this section we present a numerical simulation of a shock formation and shock propagation for a perfect gas in plane geometry. The equation of state reads

$$P(\rho, s)=e^s\rho^\gamma, \tag{6.1}$$

where $\gamma=\frac{5}{3}$ and s is the entropy per barion which is defined within an additive constant. We choose the initial conditions

$$s(x, 0)=0, \tag{6.2}$$

$$\rho(x, 0)=e^{-4x^2}+0.2, \tag{6.3}$$

$$v(x, 0)=0, \tag{6.4}$$

with the boundary conditions

$$v(a, t) = v(b, t) = 0, \tag{6.5}$$

where x lies in the range $[0, 2]$.

We present the results of a calculation performed with 2×65 grid points. The time step is constant in time and is chosen in such a way that the error on the solution is acceptable (namely 50 time steps until the shock forms). We want to emphasise that the time step is determined by a precision criterion and not by numerical stability considerations. The CPU time, which is proportional to the number of degrees of freedom, is in this case (2×65 grid points) 0.29 s per time-step on a VAX-8600 in double precision. The entire calculation was performed within 40 s of CPU time.

Figures 3a–d represent density profiles and corresponding velocity fields at successive instants: at the beginning (Fig. 3a) of the evolution; when the density and velocity gradients become steeper and steeper (Fig. 3b); when the shock forms (Fig. 3c); and, finally, when the shock propagates through the box until it reaches the wall (Fig. 3d). The sticks at the bottom of the figures show the corresponding positions of the grid matching point α.

Before the shock forms, $\dot{\alpha}(t)$ is computed as described in Section 4. When the shock forms, the initial velocity of the shock v_s is given by analytical continuation of one of the Rankine–Hugoniot relations, e.g.,

$$v_s(t_{\text{shock}}) = \lim_{x \to \alpha} \frac{\partial(\rho v)/\partial x}{\partial \rho/\partial x} \, (t = t_{\text{shock}}). \tag{6.6}$$

At $t = t_{\text{shock}}$, the spatial derivatives of the quantities become infinite on α, and, consequently, the previous relation does not have any numerical meaning. We then use for the computation of $\dot{\alpha}(t_{\text{shock}})$ the following approximation:

$$\dot{\alpha}(t_{\text{shock}}) = \frac{\partial(\rho v)/\partial x}{\partial \rho/\partial x} \, (t = t_{\text{shock}} - dt, \, x = \alpha). \tag{6.7}$$

For $t > t_{\text{shock}}$, $\dot{\alpha}$, which is now the velocity of the shock, is computed by means of the mass conservation through the shock. Numerically speaking, the problem of infinite derivatives remains during a small interval of time Δt. To avoid this

FIG. 3. Density profiles and velocity fields for successive time steps starting with the initial conditions given by Eqs. (6.1)–(6.5). (a) The fluid moves from left to right. The sticks at the bottom of the figures show the position of the matching point $\alpha(t)$; (b) Continuation of Fig. 3a. Note that the density and the velocity profiles become steeper and steeper. The matching point $\alpha(t)$ becomes closer and closer to the point of maximum gradient. (c) Continuation of Fig. 3b. Birth of the shock. When the shock is formed, the sticks show the position of the matching point $\alpha(t)$ which is now the shock position. From now, entropy is produced by the shock (see Fig. 4). (d) Continuation of Fig. 3c. The shock is now propagating toward the wall of the box. The calculation is stopped when the shock reaches the wall because the code is not able to handle the physics of the wall.

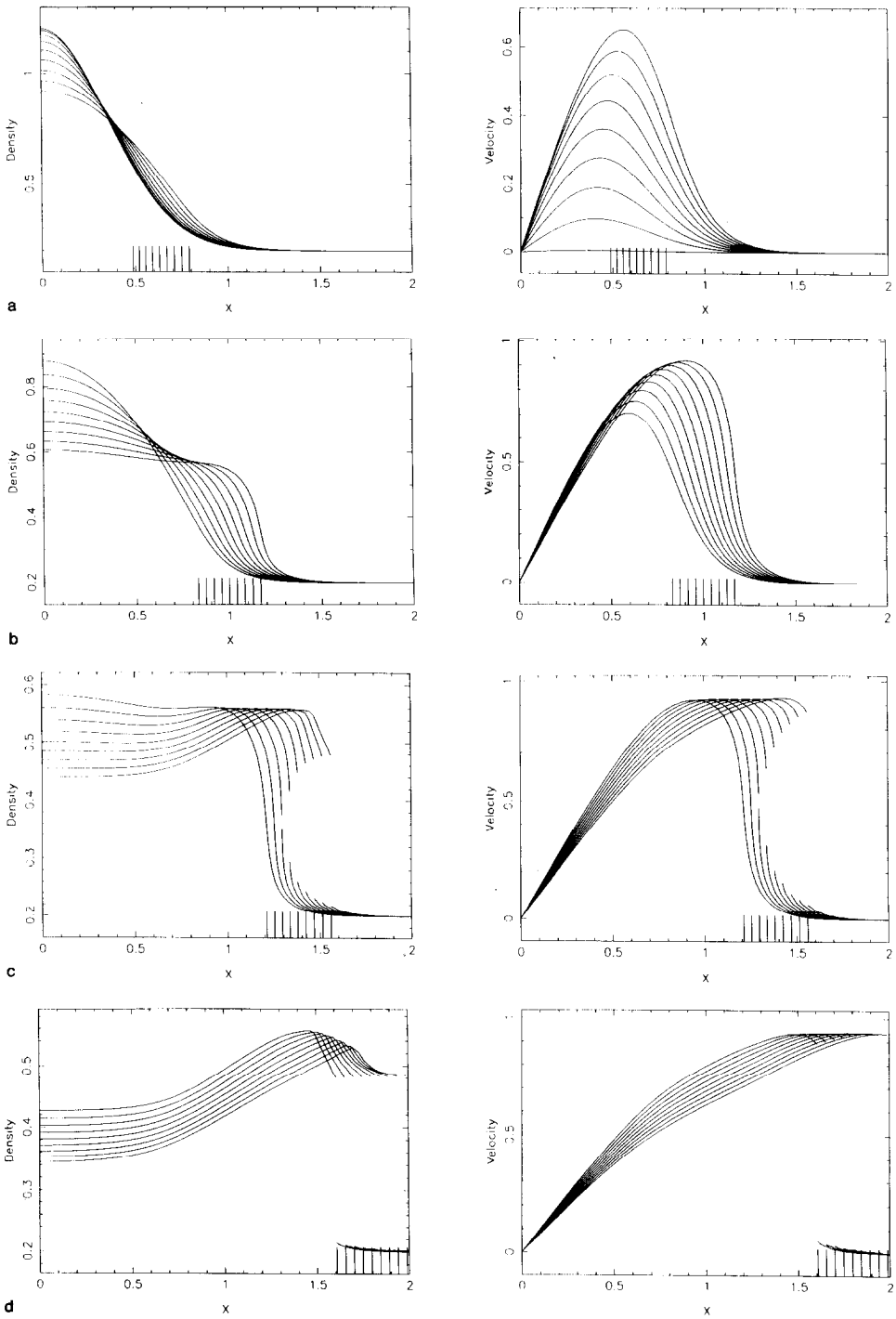
Density
Velocity
x
a
b
c
d

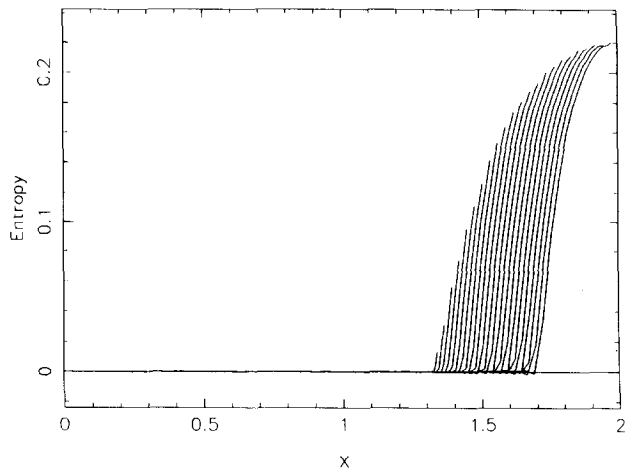

FIG. 4. Profiles of the entropy at successive time steps for all the calculation. Note that the entropy remains constant before the birth of the shock.

problem we modify the density and the velocity values (only) at the time of the shock formation on the shock location by computing the values of $\rho(\alpha^+)$, $\rho(\alpha^-)$, $v(\alpha^+)$, and $v(\alpha^-)$ in such a way that the curvature of the above quantities at $x=\alpha^+$ and $x=\alpha^-$ vanishes. This numerical trick (which is the only one in the entire calculation) is, of course, not unique. There are a few other possibilities which we tried. All these tricks gave the same practical results. It is to be noticed that the artificial modification we introduce is just a change in the initial conditions of the calculation after the shock formation.

TABLE I

Quantity	Domain of validity	Lower bound of error	Upper bound of error
$\frac{\rho(\alpha^+)}{\rho(\alpha^-)}-1$	$t \leqslant t_{\text{shock}}$	-1.5×10^{-15}	$+1.2\times10^{-15}$
$\frac{v(\alpha^+)}{v(\alpha^-)}-1$	$t \leqslant t_{\text{shock}}$	-1.0×10^{-14}	$+2.0\times10^{-13}$
$\frac{\partial\rho/\partial x(\alpha^+)}{\partial\rho/\partial x(\alpha^-)}-1$	$t \leqslant t_{\text{shock}}$	-2.0×10^{-2}	$+4.0\times10^{-2}$
$\frac{\partial v/\partial x(\alpha^+)}{\partial v/\partial x(\alpha^-)}-1$	$t \leqslant t_{\text{shock}}$	-2.0×10^{-2}	$+3.0\times10^{-2}$
R.H. rel. on mass	$t \geqslant t_{\text{shock}}$	-1.4×10^{-17}	$+1.4\times10^{-17}$
R.H. rel. on momentum	$t \geqslant t_{\text{shock}}$	-4.0×10^{-9}	$+2.0\times10^{-9}$
R.H. rel. on energy	$t \geqslant t_{\text{shock}}$	-1.0×10^{-8}	$+3.0\times10^{-8}$

The entropy production is computed by means of the Rankine–Hugoniot relation relative to the non-accumulation of energy on the shock. The entropy profiles after the shock is formed are presented in Fig. 4. We do not present the entropy profiles for $t < t_{\text{shock}}$ because s remains constant in space and time. The gaps of the density ρ and the temperature $T = \kappa P/\rho$ as function of time are shown in Figs. 5a–b.

In the presented calculation the total mass and the total energy have to be

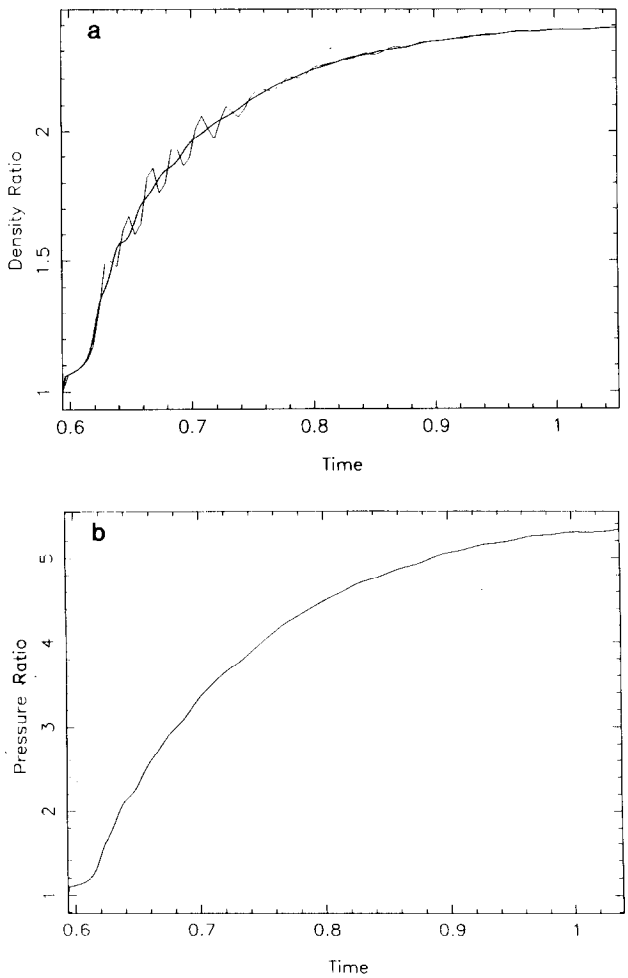

FIG. 5. (a) Plot of $\rho(\alpha^+)/\rho(\alpha^-)$ as a function of time since the shock is formed (heavy line). The light line represents the same quantity obtained with a time step four times larger than in the previous case. The oscillations on the light line are due to the errors introduced in the Rankine–Hugoniot relations by the time discretization. However, the stability of the shock together with the stability of the numerical scheme introduce a feedback compensating the errors. The small gap at $t = t_{\text{shock}}$ is due to the trick used to handle the infinite derivatives of the quantities at the birth of the shock (see Section 6). (b) Plot of $P(\alpha^+)/P(\alpha^-)$ as a function of time since the shock is formed.

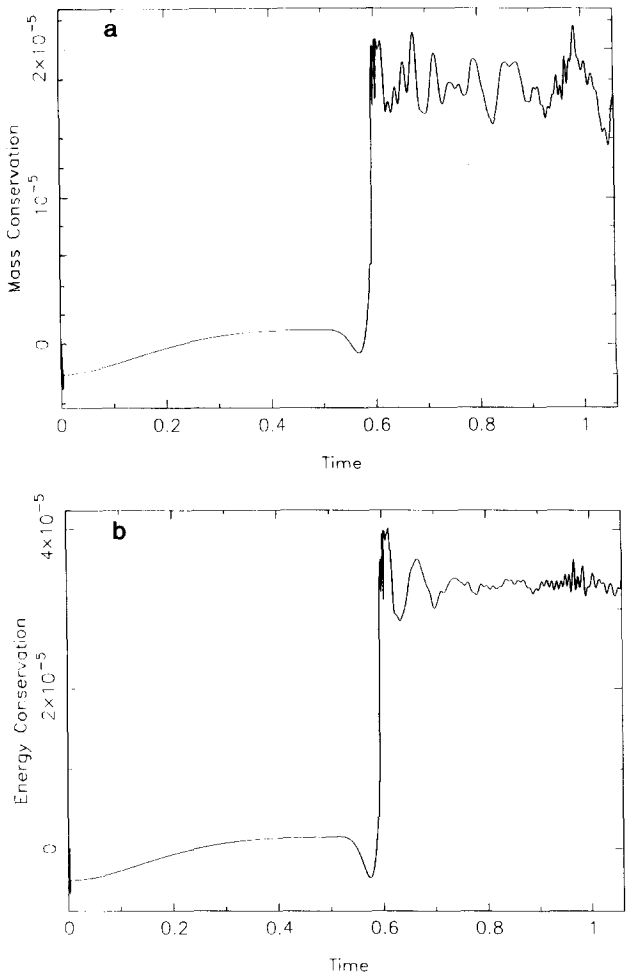

FIG. 6. (a) Relative error on the mass conservation as function of time. The trick which we used to handle the infinite derivatives at the birth of the shock is responsible of the growing of the error at this moment. (b) Relative error on the energy conservation as function of time.

conserved. Figures 6a–b show the relative error in these conservation laws as a function of time.

Table I present numerical error bounds on the matching errors when no shock is present and on the Rankine–Hugoniot conditions when shock is present.

7. CONCLUSION

We have presented a numerical technique that is able to solve Euler equations with a general equation of state with or without shock formation. No artificial

viscosity is used. The physical space is spanned by means of two moving numerical grids. When no shock is present, the equation of motion of the grids is computed in such a way that the matching point becomes the shock location when the shock forms. When the shock propagates, the equation of motion of the grid is given by one of the Rankine–Hugoniot relations.

The numerical method is based on pseudo-spectral methods, each quantity being expanded in Chebychev polynomial series on both the numerical grids. This technique allows numerical solutions with the great accuracy typical of spectral methods. In particular, it has been shown that the conservation laws are satisfied with a high accuracy depending essentially on the time step. Since the code does not use any kind of viscosity and since there is no spatial diffusion because of the spectral methods, the small amount of losses of conserved quantities is generated by the time discretisation.

We have shown that the numerical technique allows easy treatment of matching conditions before and after the shock formation. However, a problem arises at the moment of the shock formation where spatial derivatives become infinite on the matching point and where the Rankine–Hugoniot relations cannot be numerically used to compute the initial velocity of the shock. We then used at this moment a numerical trick which is more or less satisfactory.

The method can be generalized to multi-shock cases in a straightforward but cumbersome way. However, the direct generalization of the method to the multi-dimensional case can be performed only when the shape of the surface of the shock is not too complicated.

A version of this code which takes into account the regularity properties of the scalar and the vector fields in the case of spherical geometry in now in progress. This version will be used to study 1D gravitational collapse of the core of a star with the most complete equation of state. We recall that for this problem, high accuracy is needed because the energy emitted during the collapse of a star is only a few per thousand of the energy involved. This code will be the standard code which will be used to estimate the influence of the numercial viscosity present in the 2D and 3D gravitational codes.

ACKNOWLEDGMENTS

We thank A. Mangeney for many useful discussions. We are grateful to Brandon Carter, F.R.S., for a careful reading of the drafts of this paper. We thank also the ITP at Santa Barbara for their hospitality where this work was started. We want to acknowledge the staff of the S.I.O. of the Observatoire de Meudon where the numerical simulations presented in this paper have been achieved on a VAX-8600. We are grateful to Madame Lazareff who has kindly drawn Figs. 1 and 2.

REFERENCES

1. R. D. RICHTMYER AND K. W. MORTON, *Difference Methods for Initial Value Problems* (Interscience, New York, 1967).
2. S. BONAZZOLA AND J. A. MARCK, *Astron. Astrophys.* **164**, 300 (1986).

3. S. Bonazzola and J. A. Marck, *J. Comput. Phys.* **87**, 201 (1990).
4. M. G. Macaraeg and C. L. Streett, NASA Technical Memorandum 87701, 1986 (unpublished).
5. M. Y. Husaini *et al.*, *AIAA J.* **23**, 234 (1985).
6. B. E. McDonald, *J. Comput. Phys.* **82**, 413 (1989).
7. E. Tadmore, *SIAM J. Numer. Anal.* **26**, 30 (1989).
8. T. D. Taylor *et al.*, *Comput. Fluids* **9** (1981).
9. S. K. Godunov, *Mat. Sb.* **47**, 271 (1959).
10. P. Glaister, *J. Comput. Phys.* **74**, 382 (1988).
11. J. M. Marti *et al.*, *Astron. Astrophys.* **235**, 535 (1990).
12. P. Lefloch and P. A. Raviar, *Ann. Inst. Henri Poincaré* **5**, 179 (1988).
13. K. Dang *et al.*, *Rech. Aérosp.* **5**, 315 (1986).
14. D. Gottlieb and S. Orszag, *Numerical Analysis of Spectral Methods: Theory and Application*, Regional Conference Series in Applied Mathematics, Vol. 26 (Soc. Indus. Appl. Math., Philadelphia, 1977).
15. C. Canuto, M. Y. Hussaini, A. Quarteroni, and T. A. Zang, *Spectral Methods in Fluid Dynamics* (Springer-Verlag, New York/Berlin, 1988).